

# High-Power All-Solid Secondary Battery with High Heat Resistance

Takashi UEMURA\*, Kazuhiro GOTO, Mitsuyasu OGAWA and Keizo HARADA

We have developed an all-solid lithium-ion secondary battery consisting of a sulfide-based thin film electrolyte and pellet-type electrodes. The safety of lithium-ion batteries is significantly increased by replacing the electrolyte solutions with flame-retardant solid electrolytes. This battery has high performance characterized by a high discharge rate and excellent high-temperature cycle property. The battery showed a discharge capability of 10 C for one minute and capacity maintenance rates of 90% after 1500 cycles at 60°C, 90% after 500 cycles at 80°C, and 70% after 500 cycles at 150°C. We conclude that the thin film electrolyte has improved both the discharge rate and high-temperature cycle performance.

Keywords: all-solid secondary battery, sulfide-based thin film, discharge rate, high-temperature cycle performance

## 1. Introduction

Secondary batteries are widely used to power mobile electronic devices and other equipment, and extensive research has led to the development of lithium-ion batteries with a high energy density. As a larger number of vehicles use lithium-ion batteries, it has become increasingly important to improve their safety. However, lithium-ion batteries, which use combustible organic electrolyte solutions, have ignition and explosion risks. To address this problem, efforts are currently underway to significantly increase the safety of lithium-ion batteries by replacing the electrolyte solutions with flame-retardant electrolytes<sup>(1)-(3)</sup>. Among others, the all-solid lithium secondary battery is receiving particular attention as a next-generation rechargeable battery. This battery has a high thermal stability from room temperature to 360°C<sup>(3)</sup> and operates with Li<sub>2</sub>S-P<sub>2</sub>S<sub>5</sub> sulfide solid electrolytes that have a high lithium ion conductivity of at least 1×10<sup>-3</sup> S/cm at room temperature<sup>(4)</sup>. However, the all-solid battery using no organic electrolyte solution has problems as follows: it is difficult to secure a wide contact area at the interface between the active material and electrolyte; and it has a high interface resistance due to the significantly low mobility of lithium ions at the contact interface between the cathode material and solid electrolyte, which negatively affects the power density of the battery<sup>(5)-(7)</sup>. The former is particularly serious with bulk-type all-solid batteries; a strong press force needs to be applied to the electrode during the evaluation, which has been an obstacle to their practical use. For the latter, on the other hand, you can effectively reduce the interface resistance by coating the cathode with a film made of a lithium-ion conductive oxide to create a buffer layer (interlayer)<sup>(8)</sup>. Thinning the solid electrolyte layer between the positive and the negative electrodes to reduce the interface resistance also effectively improves the charge and discharge performance. We produced a prototype all-solid-state battery consisting of laminated layers of positive- and negative-electrode materials and a solid electrolyte. The solid electrolyte thin film layer of the battery maintained its performance during 500 cycles of charging and discharging<sup>(9)-(11)</sup>. An all-solid-state

lithium battery using a sulfide thin-film electrolyte as its separator for the powder composite electrode was also reported<sup>(12)</sup>.

Our prototype all-solid battery has a new structure consisting of a sulfide solid electrolyte film made by the vapor-phase method between the bulk electrodes made of several types of powders. Applying the thin film electrolytes to the cathode and anode before attaching electrodes reduced defects that penetrate through the electrolyte layer. Additionally, the rocking-chair type active material was used on both electrodes. As a result, short circuiting was reduced, and we succeeded in achieving a high discharge rate and high performance (at a high temperature). This paper reports on the assessment results.

## 2. Experimental

### 2-1 Preparation of electrode materials

Commercially available LiNi<sub>0.8</sub>Co<sub>0.15</sub>Al<sub>0.05</sub>O<sub>2</sub> and 2 wt% carbon-added Li<sub>4</sub>Ti<sub>5</sub>O<sub>12</sub> were used as the cathode and anode materials, respectively, and Li<sub>2</sub>S-P<sub>2</sub>S<sub>5</sub> glass ceramic powder was used as a solid electrolyte. Mixtures of active materials and solid electrolyte powders were used as electrode materials: an 80Li<sub>2</sub>S-20P<sub>2</sub>S<sub>5</sub> solid electrolyte with an Li:P molar ratio of 8:2 or a 70Li<sub>2</sub>S-30P<sub>2</sub>S<sub>5</sub> solid electrolyte with an Li:P molar ratio of 7:3 was used for the positive electrode, and a 70Li<sub>2</sub>S-30P<sub>2</sub>S<sub>5</sub> solid electrolyte for the negative electrode. The synthetic condition of these electrolyte powders is shown in previous reports<sup>(13)</sup>.

The cathode materials contained in all samples were coated with LiNbO<sub>3</sub>, which serves as an intermediate layer. The layer was created using Coating Equipment for Rolling Fluidized Beds MP-01 (Powrex Corp.) - the same method reported in a study conducted by Takada et al<sup>(8)</sup>. An alkoxide solution of metallic elements was used as the material for the intermediate layer; an ethanol solution containing 5 wt% of lithium ethoxide (structural formula: Li(OC<sub>2</sub>H<sub>5</sub>)) was used as the lithium source; pentaethoxyniobium (structural formula: Nb(OC<sub>2</sub>H<sub>5</sub>)<sub>5</sub>, purity of 4N) was used as the niobium

source. A mixture of an ethanol solution containing 5 wt% of lithium ethoxide and pentaethoxyniobium with a prescribed ratio was sprayed at 500 g of  $\text{LiNi}_{0.08}\text{Co}_{0.15}\text{Al}_{0.05}\text{O}_2$  poured into the equipment at a temperature of  $80^\circ\text{C}$  at 1 g/min to provide the coating, which then underwent heat treatment for 30 minutes at  $300^\circ\text{C}$  to create the intermediate layer of  $\text{LiNbO}_3$ . Inductively Coupled Plasma Atomic Emission Spectroscopy (ICP-AES) was performed to determine the ratio of elements contained in the intermediate layer and cathode material. Field Emission Auger Electron Spectroscopy (FE-AES) was also performed to examine changes in the particle surface during the coating process by using an electron gun with an accelerating voltage of 10 keV. All of the batteries used for electrochemical measurements were made from this  $\text{LiNi}_{0.08}\text{Co}_{0.15}\text{Al}_{0.05}\text{O}_2$ . No intermediate layer was formed in the anode material.

### 2-2 Preparation and evaluation method of battery

Mixtures of active material powder and sulfide electrolyte powder were pressed into a mold in a dry room set at the dew point of  $-55^\circ\text{C}$  or lower. The electrodes were cut cross-sectionally using a focused ion beam system to observe the inside with scanning ion microscopy (FIB-SIM). The electrodes for the batteries were prepared except for the electrodes for the analysis of FIB and SIM. When creating electrodes, aluminum plates were also pressed as power collectors.

The solid electrolyte film was formed on both the positive and negative bulk electrodes. Using a vacuum deposition below 0.005 Pa, a  $5\text{-}\mu\text{m}$  solid electrolyte film was formed, using  $\text{Li}_2\text{S}$  and  $\text{P}_2\text{S}_5$  as the starting materials. The positive and negative electrodes were pressed together to be integrated at the sulfide solid electrolyte film sides. The bulk electrolytes were attached together over an area of  $\varnothing 10\text{ mm}$ , based on which the density of the battery capacity was calculated.

Only constant-current, charge-discharge tests were conducted to examine the discharge rate and characteristics of the batteries. The alternating-current impedance was measured using an analyzer before and after charging at the alternating-current amplitude of 10 mV and the frequency range of 10 mHz to 100 kHz.

## 3. Results and Discussion

### 3-1 Evaluation of electrode

After coating the cathode powder  $\text{LiNi}_{0.08}\text{Co}_{0.15}\text{Al}_{0.05}\text{O}_2$  with  $\text{LiNbO}_3$ , an intermediate layer, ICP analysis was conducted to determine the element ratio; the weight of Ni and Nb contained in 100 mg of coated powder was 48 and 0.85 mg, respectively. The mean thickness was 7.2 nm, which was calculated based on a specific surface area of the powder ( $0.41\text{ m}^2/\text{g}$ ) determined by the conventional gas absorption method and the theoretical density of the intermediate layer. From the results of the element mapping shown in Fig. 1, which were obtained using Auger spectroscopy, the surface coverage of the intermediate layer  $\text{LiNbO}_3$  was estimated to be approximately 80%. Previous studies reported that, regarding all-solid batteries, the thickness of the intermediate layer  $\text{LiNbO}_3$  or  $\text{Li}_4\text{Ti}_5\text{O}_{12}$  for

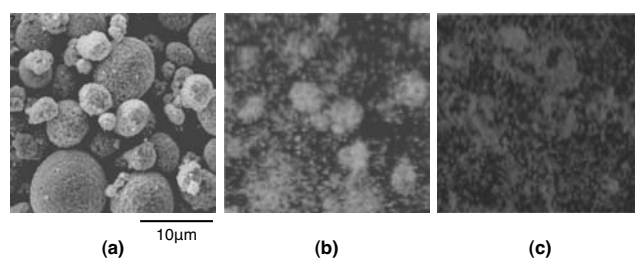


Fig. 1. SEM images of  $\text{LiNi}_{0.08}\text{Co}_{0.15}\text{Al}_{0.05}\text{O}_2$  powder after coating with the  $\text{LiNbO}_3$  intermediate layer: (a) Auger electron spectroscopy mapping, (b) Nb mapping image, (c) Ni mapping image

the cathode material  $\text{LiCoO}_2$  should be 5 to 7 nm<sup>(5),(6)</sup>, and the intermediate layer  $\text{Li}_4\text{Ti}_5\text{O}_{12}$  for  $\text{LiNi}_{0.08}\text{Co}_{0.15}\text{Al}_{0.05}\text{O}_2$  should be approximately 5 nm<sup>(8)</sup>. The thickness of the intermediate layer  $\text{LiNbO}_3$  for  $\text{LiNi}_{0.08}\text{Co}_{0.15}\text{Al}_{0.05}\text{O}_2$  reported in the present study is in line with the results of previous studies.

The FIB-SIM sectional images, in Fig. 2, show that the inside of the molded electrodes was densely packed and accordingly the cathode and anode materials were closely contacted with the solid electrolytes. Primary particles of 1  $\mu\text{m}$  or smaller and secondary particles of approximately 6  $\mu\text{m}$  were observed in both active materials. Even-grain boundaries were barely visible between the solid electrolyte particles, and the contact resistance was considered to be markedly low.

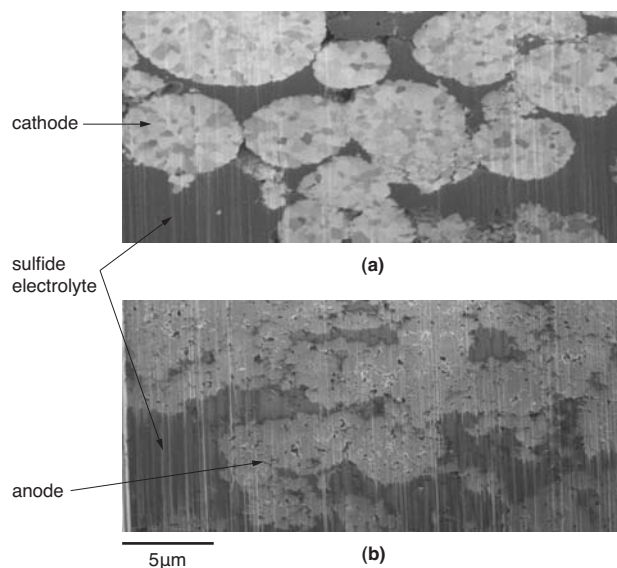


Fig. 2. FIB-SIM sectional images of the molded electrodes: (a) positive electrode, (b) negative electrode

### 3-2 Charge and discharge performance

An examination was conducted to investigate the charge and discharge characteristics of the battery that used an  $80\text{Li}_2\text{S}-20\text{P}_2\text{S}_5$  solid electrolyte as its positive-electrode material and a  $70\text{Li}_2\text{S}-30\text{P}_2\text{S}_5$  solid electrolyte as its

negative-electrode material. The battery was charged at 0.1 C ( $0.3 \text{ mA/cm}^2$ ) at  $25^\circ\text{C}$ , and discharged at a different current value. **Figure 3** shows the results - the horizontal was normalized by the weight of the positive active material. With a high current density of 10 C ( $30 \text{ mA/cm}^2$ ), the battery discharged for 15 seconds, and the discharge capacity was  $6.4 \text{ mAh/g}$ .

The battery that used  $70\text{Li}_2\text{S-}30\text{P}_2\text{S}_5$  solid electrolytes for both positive- and negative-electrode materials was charged at  $25^\circ\text{C}$  at 0.1 C ( $0.3 \text{ mA/cm}^2$ ), and discharged at a different current value. **Figure 4** shows the results. At the time of discharge at a high rate (5 or 10 C), the battery capacity was high compared to that of a battery using an  $80\text{Li}_2\text{S-}20\text{P}_2\text{S}_5$  solid electrolyte on the positive electrode side: the battery was able to discharge for 1 minute at 10 C ( $0.3 \text{ mA/cm}^2$ ), and the discharge capacity was  $25.7 \text{ mAh/g}$ . The solid electrolyte in the form of pressurized powder was examined to measure its ionic conductivity. The ionic conductivity of a  $70\text{Li}_2\text{S-}30\text{P}_2\text{S}_5$  pellet was  $1 \times 10^{-3} \text{ (S/cm)}$ , higher than that of an  $80\text{Li}_2\text{S-}20\text{P}_2\text{S}_5$  pellet:  $4 \times 10^{-4} \text{ (S/cm)}$ , suggesting an increase in capacity.

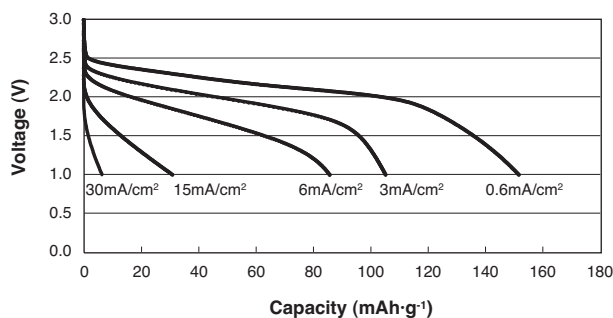


**Fig. 3.** Discharge curves at various current densities of the battery that used an  $80\text{Li}_2\text{S-}20\text{P}_2\text{S}_5$  solid electrolyte as positive-electrode and a  $70\text{Li}_2\text{S-}30\text{P}_2\text{S}_5$  solid electrolyte as negative-electrode

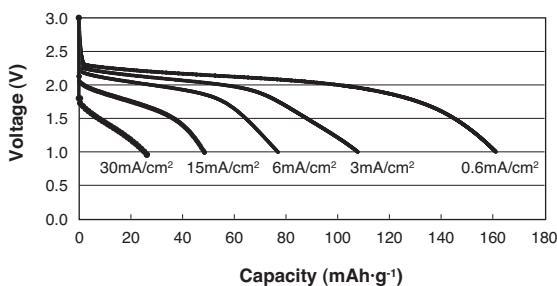


**Fig. 4.** Discharge curves at various currents of the battery that used a  $70\text{Li}_2\text{S-}30\text{P}_2\text{S}_5$  solid electrolyte as both positive and negative electrodes

### 3-3 Cycle performance at high temperature

The battery that used an  $80\text{Li}_2\text{S-}20\text{P}_2\text{S}_5$  solid electrolyte as its positive-electrode material and a  $70\text{Li}_2\text{S-}30\text{P}_2\text{S}_5$  solid electrolyte as its negative-electrode material was packaged

into a 2032 coin cell. **Figure 5** shows the results of a charge-discharge test for the coin cell battery. The coulomb efficiency in the first and second cycles was 73% and 94%, respectively, and the discharge capacity was  $148 \text{ mAh/g}$ . Except for the package case, the battery was fabricated by the same process as the battery shown in **Fig. 3**. The slight difference of the capacity between **Fig. 3** and **Fig. 5** is attributed to the small difference in the dispersion of active material powder in the electrodes.

The battery was repeatedly charged and discharged by applying a 3V-1V cut-off voltage at  $60^\circ\text{C}$  and  $3 \text{ mA/cm}^2$ . **Figure 6** shows the capacity change during the charge and discharge cycle. The discharge capacity was highest,  $149 \text{ mAh/g}$  (100%), in the fifth cycle,  $143 \text{ mAh/g}$  (96%) at the end of the 500th cycle,  $137 \text{ mAh/g}$  (92%) at the end of the 1,000th cycle, and  $134 \text{ mAh/g}$  (90%) at the end of the 1,500th cycle.

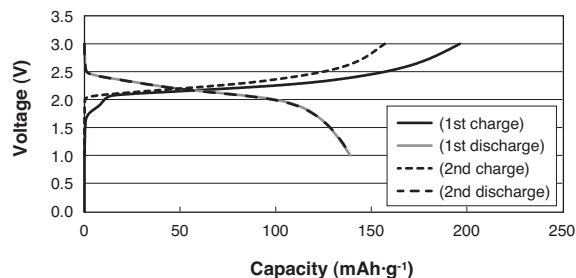


**Fig. 5.** Charge-discharge performance of the coin cell battery

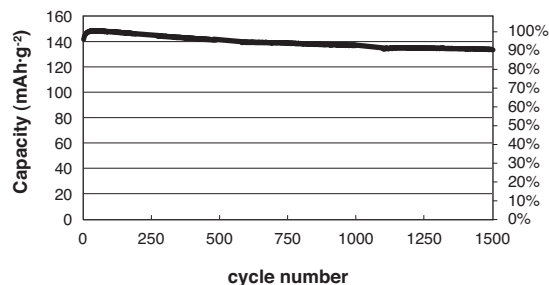


**Fig. 6.** Charge-discharge performance of the coin cell at  $60^\circ\text{C}$

**Figure 7** shows detailed information on the discharge rate property at a room temperature. The battery was the same as that shown in **Figs. 6 and 7**. The discharge capacity was measured after cooling to room temperature at the end of the 500th cycle and 1,000th cycle at  $60^\circ\text{C}$ . As a result, the capacity at a discharge current of  $3 \text{ mA/cm}^2$  declined to approximately 60% of the initial capacity after the 1,000th cycle.

The Nyquist plot in **Fig. 8** shows impedance measured immediately after the evaluation of the discharge capacity; there were no significant changes in the resistance component:  $R_1$ , and a moderate increase in the resistance compo-

nent:  $R_2$ . It was appropriate to consider that the resistance component at higher frequencies ( $R_1$ ) was the resistance of the solid electrolyte, and that the resistance component at lower frequencies ( $R_2$ ) was a charge-transfer reaction at the interface. However, the resistance of the electrolyte was estimated to be below  $3 \text{ ohm}\cdot\text{cm}^2$  from the ionic conductivity and thickness of the electrolyte layer. The estimated value was smaller than the measured  $R_1$ . This difference can be attributed to the addition of the electronic resistance of the battery in  $R_1$  value. In detail,  $R_2$  seems to consist of two capacitance components, and the resistance of the higher frequency component increased after the cycle test.  $R_2$  of the battery using  $\text{LiNbO}_3$  non-coated positive active material was ten times larger than that of the battery shown in Fig. 8. It is supposed that the two components of  $R_2$  belong to the two interfaces of cathode/electrolyte and anode/electrolyte. This suggests that the cause of the decrease in discharge capacity was the increased resistance in the active material and at the interface of the solid electrolyte and that the ionic conductivity of the solid electrolyte film remained as it was at the initial state. Previous studies on degradation mechanisms at high temperature report that different phases are formed at the interface between the cathode material and the sulfide solid electrolyte, which significantly increases the

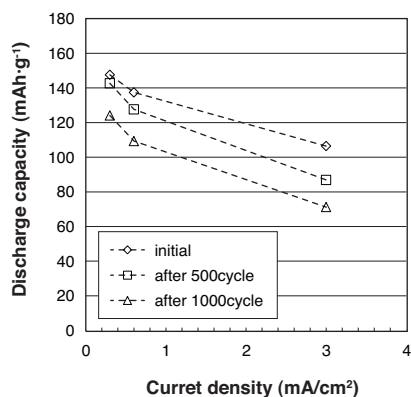


Fig. 7. Discharge capacity at 25°C after 60°C charge-discharge cycles

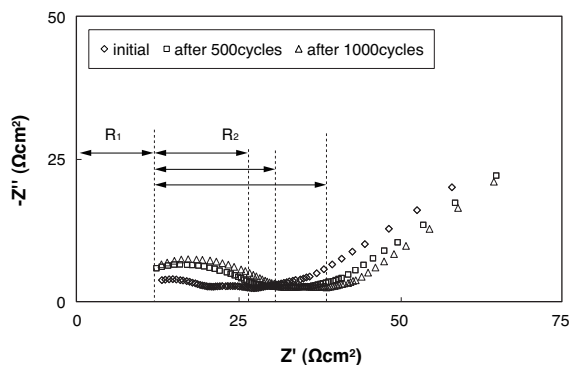


Fig. 8. Nyquist plot measured at 25°C after 60°C charge-discharge cycles

interface resistance<sup>(14)</sup>.

To examine the formation of different phases at the interface, a battery with the same structure as above-mentioned was charged and discharged 500 times at 60°C, and TEM-EDX analysis was conducted for the interface between the cathode material and solid electrolyte. As shown in Fig. 9, there was no different phase at the interface, although a small amount of oxygen was observed at the interface of the solid electrolyte. The initial sample fabricated by the process presented in Fig. 9 showed no oxygen at the interface of the solid electrolyte, according to the TEM-EDX analysis. Therefore, it was supposed that oxygen at the interface dispersed from the active material. Oxygen was released from the active material which became unstable because the cathode materials were partly overcharged. The oxygen dispersion at the interface was considered to have increased the resistance component  $R_2$  and decreased the discharge capacity following the cycle test at 60°C. The formation of an inter-particle void due to a change in the volume of the active material during the charge-discharge cycle was also considered to be a physical factor related to an increase in the resistance at the interface. However, since the change in the volume of the anode material  $\text{Li}_4\text{Ti}_5\text{O}_{12}$ , in particular, was only 0.2% when the SOC was between 0 to 100%<sup>(15)</sup>, chemical degradation was the primary cause.

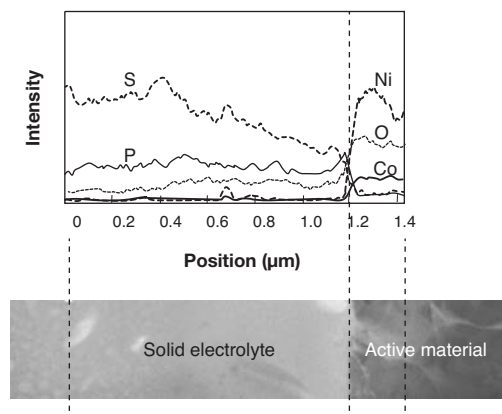
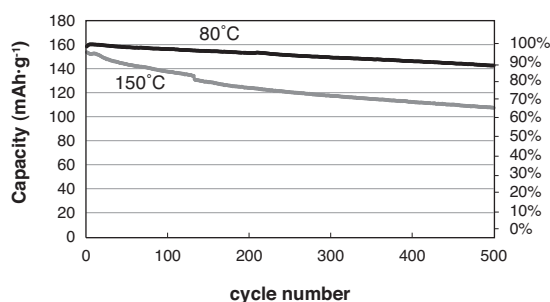


Fig. 9. TEM-EDX analysis of the interface between  $80\text{Li}_2\text{S}-20\text{P}_2\text{S}_5$  solid electrolyte and  $\text{LiNi}_{0.8}\text{Co}_{0.15}\text{Al}_{0.05}\text{O}_2$  after the 500th cycle at 60°C

No previous studies reported that the high discharge rates and long-term cycle characteristics shown in Figs. 6 and 7 could be compatible, although a moderate level of high-temperature degradation was noted. This compatibility was achieved because the volume of the active material did not significantly change during the charge-discharge cycle, and the electrodes and solid electrolyte films created using the vacuum evaporation method were dense.

A test involving an all-solid battery that used an  $80\text{Li}_2\text{S}-20\text{P}_2\text{S}_5$  solid electrolyte on the positive side was also conducted to examine changes in its discharge capacity while the battery was charged and discharged 80 times at 150°C.

In the cycle test, the current value was 3 mA/cm<sup>2</sup> and the cut-off voltage was 3V-1V when the temperature was 80°C; and the current value was 9 mA/cm<sup>2</sup> and the cut-off voltage was 2.7V-1V when the temperature was 150°C. **Figure 10** shows the results of the test conducted at high temperature. The initial discharge capacity was 158 mAh/g (100%) and 142 mAh/g (90%) at the end of the 500th cycle when the temperature was 80°C, and the initial discharge capacity was 155 mAh/g (100%) and 108 mAh/g (70%) at the end of the 500th cycle at 150°C, which suggests that the battery has a driving power of 500 charge-discharge cycles at 150°C.



**Fig. 10.** Charge-discharge cycle performance of the coin cell at 80°C and 150°C

#### 4. Conclusion

In recent years, several advanced studies have reported that all-solid batteries have the ability to discharge at a high current density<sup>(8),(16)</sup>. The battery examined in the present study demonstrated a high capacity and a high discharge rate at room temperature and favorable cycle characteristics compared to the batteries reported in previous studies. Although several studies have been conducted to examine the heat resistance of all-solid batteries depending on their constituents, there are few reports on the integrated driving characteristics of these batteries. The present study demonstrated that all-solid batteries can be charged and discharged 500 times in a harsh temperature environment of 150°C. These battery characteristics were achieved by reducing the interface resistance with the intermediate layer coating for a cathode material and reducing the bulk resistance using a thin film as a solid electrolyte layer.

#### References

- (1) K. Takada, N. Aotani, K. Iwamoto, S. Kondo, *Solid State Ionics* 86 (1996) 877-882.
- (2) R. Hagiwara, K. Tamaki, K. Kubota, T. Goto, T. Nohira, *J. Chem. Eng. Data*, 53 (2008) 355.
- (3) A. Hayashi, *J. Ceram. Soc. Jap.* 115 (2007) 110-117.
- (4) N. Kayama, K. Homma, Y. Yamakawa, M. Hirayama, R. Kanno, M. Yonemura, T. Kamiyama, Y. Kato, S. Hama, K. Kawamoto, A. Mitsui, *Nature Materials* 10 (2011) 682-686.
- (5) N. Ohta, K. Takada, L. Zhang, R. Ma, M. Osada, T. Sasaki, *Adv. Mater.* 18 (2006) 2226-2229.
- (6) N. Ohta, K. Takada, I. Sakaguchi, L. Zhang, R. Ma, K. Fukuda, M. Osada, T. Sasaki, *Electrochemistry Communications* 9 (2007) 1486-1490.
- (7) K. Takada, N. Ohta, L. Zhang, K. Fukuda, I. Sakaguchi, R. Ma, M. Osada, T. Sasaki, *Solid State Ionics* 179 (2008) 1333-1337.
- (8) Y. Seino, T. Ota, K. Takada, *J. Power Sources* 196 (2011) 6488-6492.
- (9) M. Ogawa, R. Kanda, K. Yoshida, T. Uemura, K. Harada, *J. Power Sources* 205 (2012) 487-490.
- (10) N. Ota, N. Okuda, K. Emura and A. Yamakawa, *SEI technical review* 61 (2006) 41-47.
- (11) M. Ogawa, K. Yoshida and K. Harada, *SEI technical review* 74 (2012) 88-90.
- (12) A. Sakuda, A. Hayashi, T. Ohtomo, S. Hama and M. Tatsumisago, *Electrochemistry* 80 (2012) 839
- (13) F. Mizuno, A. Hayashi, K. Tadanaga and M. Tatsumisago, *Adv. Mater.* 17 (2005) 918
- (14) A. Sakuda, A. Hayashi and M. Tatsumisago, *Chem. Mater.* 22 (2010) 949.
- (15) S. Scharner, W. Weppner, P. Schmid-Beurmann, *J. Electrochem. Soc.* 146 (1999) 857-861.
- (16) A. Sakuda, H. Kitaura, A. Hayashi, K. Tadanaga, M. Tatsumisago, *Electrochem. Solid-State Lett.* 11 (2008) A1-A3.

#### Contributors (The lead author is indicated by an asterisk (\*).)

T. UEMURA\*

- Manager, Electronics & Materials R&D Labs.



K. GOTO

- Electronics & Materials R&D Labs.



M. OGAWA

- Assistant Manager, Electronics & Materials R&D Labs.



K. HARADA

- Assistant General Manager, R&D General Planning Division

